scientific reports

Check for updates

OPEN

Sea anemone *Bartholomea annulata* venom inhibits voltage-gated Na^+ channels and activates $GABA_A$ receptors from mammals

Antònia Colom-Casasnovas[1,2], Edith Garay[3], Abraham Cisneros-Mejorado[3], Manuel B. Aguilar[3], Fernando Lazcano-Pérez[2], Rogelio O. Arellano[3]✉ & Judith Sánchez-Rodríguez[2]✉

Toxin production in nematocysts by Cnidaria phylum represents an important source of bioactive compounds. Using electrophysiology and, heterologous expression of mammalian ion channels in the *Xenopus* oocyte membrane, we identified two main effects produced by the sea anemone *Bartholomea annulata* venom. Nematocysts isolation and controlled discharge of their content, revealed that venom had potent effects on both voltage-dependent Na^+ (Na_v) channels and GABA type A channel receptors ($GABA_AR$), two essential proteins in central nervous system signaling. Unlike many others sea anemone toxins, which slow the inactivation rate of Na_v channels, *B. annulata* venom potently inhibited the neuronal action potential and the Na^+ currents generated by distinct Na_v channels opening, including human TTX-sensitive ($hNa_v1.6$) and TTX-insensitive Na_v channels ($hNa_v1.5$). A second effect of *B. annulata* venom was an agonistic action on $GABA_AR$ that activated distinct receptors conformed by either α1β2γ2, α3β2γ1 or, ρ1 homomeric receptors. Since GABA was detected in venom samples by ELISA assay at low nanomolar range, it was excluded that GABA from nematocysts directly activated the $GABA_ARs$. This revealed that substances in *B. annulata* nematocysts generated at least two potent and novel effects on mammalian ion channels that are crucial for nervous system signaling.

Cnidarians are a diverse group of aquatic invertebrate animals that include jellyfishes, corals, hydrozoans, and sea anemones, among some others[1]. Some cnidarians are considered highly venomous on humans (e.g. Refs.[2–4]). This characteristic is associated with the synthesis and assembly of microscopic and sophisticated bioweapons known as nematocysts[5–7]. These extraordinary structures, are essentially, capsules that contain venom and are endowed with penetrant spines that allow effective venom administration on demand. Nematocysts are produced in specialized cells named nematocytes[5,8]. The venom contains a mixture of compounds[9] that includes proteinaceous (e.g., peptides, proteins, and enzymes) and non-proteinaceous (e.g., purines, quaternary ammonium compounds, biogenic amines, and betaines) substances[10,11], with neurotoxic effects and cytolytic activity, among others[12–19]. Nevertheless, the complex cnidarian venomous apparatus is still not fully understood. Recent studies show that venom source is not restricted to nematocysts. For instance, distinct stinging-cell structures called cassiosomes have been identified in the Rhizotomies order (scyphomedusae *Cassiopea xamachana*)[20], and sea anemones such as *Nematostella vectensis* or *Anthopleura elegantissima* have ectodermal gland cells that produce toxins[21]. Also, it has been shown that different toxins are expressed throughout the animal life span[22],

[1]Posgrado en Ciencias del Mar y Limnología, Universidad Nacional Autónoma de México, Circuito Exterior S/N, Ciudad Universitaria, C.P. 04510 Coyoacán, Mexico, Mexico. [2]Unidad Académica de Sistemas Arrecifales Puerto Morelos, Instituto de Ciencias del Mar y Limnología, Universidad Nacional Autónoma de México, Prolongación Niños Héroes s/n, Domicilio Conocido, C.P. 77580 Puerto Morelos, Quintana Roo, Mexico. [3]Departamento de Neurobiología Celular y Molecular, Instituto de Neurobiología, Universidad Nacional Autónoma de México, Boulevard Juriquilla 3001, 76230 Juriquilla, Querétaro, C.P, Mexico. ✉email: arellano.ostoa@comunidad.unam.mx; judithsa@cmarl.unam.mx

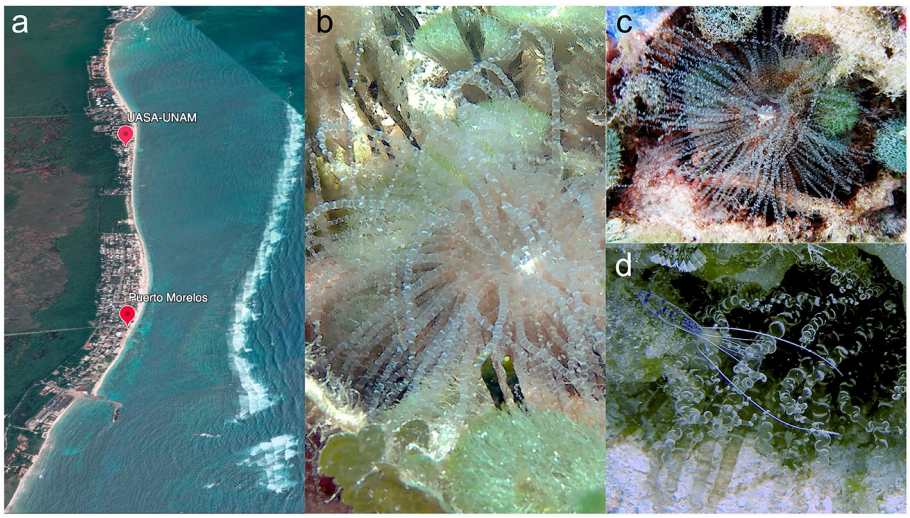

Figure 1. Sampling site location of *Bartholomea annulata* at the reef lagoon of Puerto Morelos, Quintana Roo. (**a**) Google Earth satellite image of Puerto Morelos Reef Lagoon, Quintana Roo, México; location points indicate Puerto Morelos town and the Unidad Académica de Sistemas Arrecifales UNAM (UASA-UNAM) (20° 50′ 45″ N 86° 52′ 08″ W and 20° 50′ 55″ N 86° 52′ 52″ W, respectively). (**b–d**) Sea anemone *Bartholomea annulata* is a member of family Aiptasiidae of the class Anthozoa; it is also commonly known as "corkscrew anemone", due to spiral bands on its tentacles. Regularly is found inside crevices of rocks and coral rubble and has mutualist symbiosis with the cleaner shrimp *Ancylomenes pedersoni* (**d**) and the pistol shrimp *Alpheus armatus*.

even more, different tissue types of a particular animal produce specific venom components[23]. The diversity of active substances contained in the nematocysts, and other cnidarian structures, encourages a constant search for novel, specific and potent toxins acting on vertebrate membrane proteins, especially from the nervous system. However, the number of species studied until now remains extremely low (about 4%[1]). In this search for toxins, two bottlenecks slow down new developments in the area; the first is the discovery of relevant effects and the identification of molecular targets of toxins, the second, is undoubtedly, the purification of toxins and determination of their chemical nature. In this study, we explore the toxicity of the sea anemone *Bartholomea annulata* venom and aim to determine some of its molecular targets.

Bartholomea annulata (Anthozoa:Actiniaria: Aiptasiidae: Metridiodea) is a common sea anemone that inhabits the Caribbean Sea[24–27] and produces three different types of nematocysts: basitrichous isorhizas, microbasic p-mastigophores, and microbasic amastigophores[26,28,29]. It has also been reported that *B. annulata* venom has deleterious effects on crabs, fishes, and even mice, generating spasmodic convulsions, cardiac arrhythmia, paralysis, and death[29,30]. Nevertheless, the bioactivity of *B. annulata* venom, which might explain its potent lethality, has not been directly explored on nervous system membrane proteins, in fact, venoms from the Metridioidea superfamily have been studied only in a limited number of species, one of the most comprehensive studies shows effects of *Exaiptasia diaphana* toxins acting on ion channels expressed in cardiomyocytes[31,32]. In here, we analyzed electrophysiologically the effects of *B. annulata* venom on a library of membrane proteins (from rat brain) heterologously expressed in *Xenopus* oocytes through mRNA injection. Once possible novel targets were identified, the characterization of effects was refined using various preparations for their electrophysiological analysis. We demonstrate that *B. annulata* nematocysts contain substances that produce two effects observed for the first time in the actiniarian group: (1) It potently inhibits the current flux through voltage-dependent Na^+ channels, both TTX-sensitive and TTX-insensitive channels, and (2) it acts as a GABAergic agonist activating GABA type A channel receptors ($GABA_AR$). The importance of both effects, for the central nervous system functioning, strongly suggests that these substances are central in the lethality of *B. annulata* venom and indicates the production and delivery of novel toxins from sea anemones.

Results

Bioactivity. To test bioactivity of *B. annulata* (Fig. 1) venom, either crude sea anemone extract (AE) or crude extract isolated from nematocysts (NE; see below) was administered to *Ocypode quadrata* crabs (n = 4 for each case) injecting 15–20 µg of the extract per g/crab in 50 µl PBS. In all cases, strong alterations, including tremor of legs, chelas, and eyes, uncontrolled movements, variable periods of freezing that increased until causing total paralysis, and finally death. Crabs (n = 4) injected with vehicle did not present any response. All these alterations were compatible with effects on the neuromuscular system and confirmed previous observations[29,33].

To conduct a broad screening of molecules involved in nerve transmission, we systematically analyzed the venom effect on membrane proteins from the rat brain that were heterologously expressed in *Xenopus* oocytes through mRNA injection[15,33,34]. It is well known that the oocyte has great experimental advantages for molecular target screening, including its capability to heterologously express functional proteins in its membrane that can be analyzed by electrophysiology. An example of the variety of electrical signals susceptible to analysis is shown

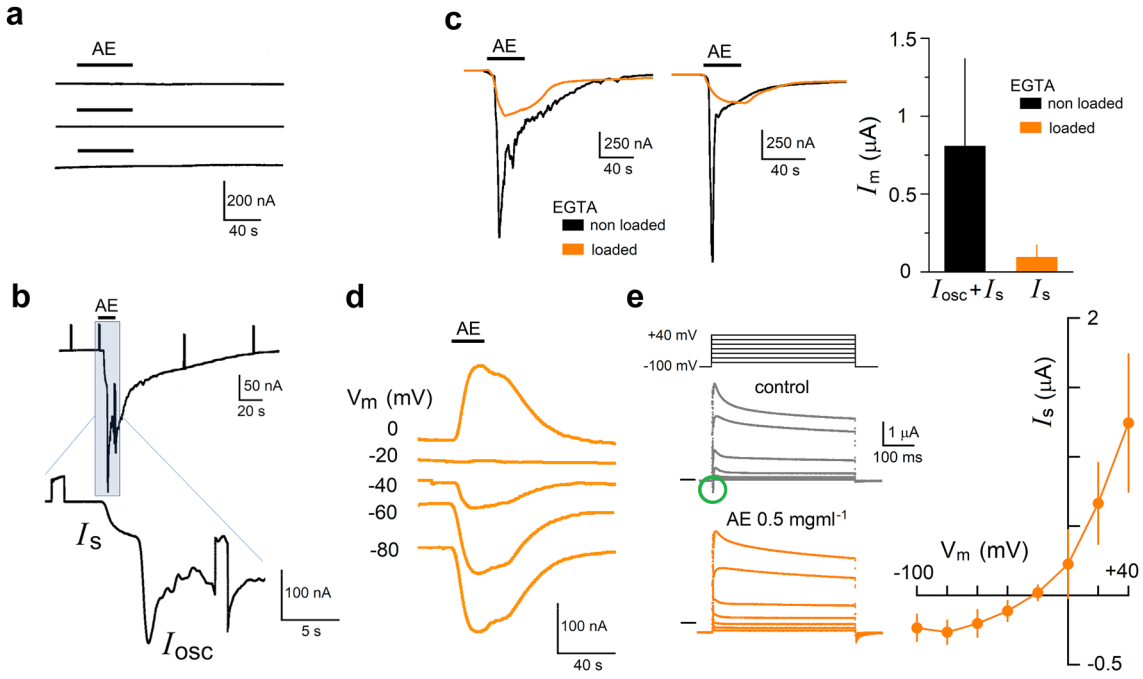

Figure 2. *Bartholomea annulata* venom produced three electrical responses in oocytes expressing membrane proteins from the rat brain. (**a**) Upper traces illustrate lack of current responses to application of anemone extract (AE, 0.1 mg ml^{-1}) in three different control H_2O-injected oocytes (3 frogs) under voltage-clamp held at − 60 mV, while in (**b**) traces show the current response elicited by AE in a mRNA-injected oocyte (expressing responses to different neurotransmitters as showed in Supplementary Fig. S1). Increase of the trace time-resolution signal in the insert (blue box) discloses activation of two currents with distinct temporal course, an early and smooth inward current, denoted I_s, and a late and oscillatory inward current, denoted I_{osc}. In (**c**) traces show that I_{osc} current observed in control response (black traces; EGTA non loaded oocytes) was eliminated in EGTA-loaded oocytes, while inward current EGTA-resistant corresponded with I_s time-course (orange traces). Total current responses (I_m) obtained in 40 control and EGTA-loaded oocytes (right graph) indicated that I_s was of 93 ± 17.7 nA (mean ± S.D.). (**d**) I_s was elicited by 0.5 mg ml^{-1} AE superfusion in mRNA-injected oocytes that were EGTA-loaded, and holding the membrane potential as indicated in each trace, it is shown that I_s reverted close to − 20 mV, similar result was obtained in 2 more oocytes from different frog. (**e**) Traces illustrate a voltage-step protocol applied in EGTA-loaded oocytes (n = 4) held at − 100 mV in the absence of AE (control, gray traces) and during the application of the venom (0.5 mg ml^{-1}; orange traces); the current–voltage relationship was built for the current elicited by AE subtracting the control current as it is shown in the graph. The black line to the left for each set of traces signals zero current. The green circle in control traces signals a fast inward current elicited at − 20 mV; this current, more probably due to opening of Na_v channels, was eliminated by AE application.

in Supplementary Fig. S1. Using mRNA-injected oocytes, AE samples from *B. annulata* were tested. Figure 2 illustrates these experiments, first AE (0.1–1 mg ml^{-1}) applied to control oocytes (H_2O-injected; Fig. 2a) did not elicit any electrical response (n = 6, 3 frogs). However, AE application in oocytes expressing brain proteins generated several electrical responses (Fig. 2b–e), particularly three effects on three different responses were observed in all the oocytes tested. Thus, in oocytes held at − 60 mV, AE generated two types of currents that can be distinguished by their time-course (Fig. 2b) and their dependency on an intracellular Ca^{2+} concentration ($[Ca^{2+}]_i$) increase (Fig. 2c). These current responses are indicated as I_s (smooth) and I_{osc} (oscillatory) in Fig. 2b. The first response, I_s, was an inward current associated with an increase in membrane conductance. The second response, I_{osc}, began to increase a few seconds later and corresponded to an inward oscillatory current associated with an increase in conductance. Both responses, were co-activated while AE perfusion was maintained and were washed completely by NR superfusion. I_{osc} resembled the typical responses to various neurotransmitters when their receptors are expressed through brain mRNA injection in the oocyte (Fig. S1[35]). These are currents dependent on $[Ca^{2+}]_i$ increase promoted by phospholipase C activation and are due to Ca^{2+}-dependent Cl^- channels opening[36,37]. To explore if I_{osc} elicited by the extract was activated through the same mechanism, oocytes that generated I_{osc} by AE, were washed, loaded with EGTA[38], and then tested again with AE (Fig. 2c, orange traces). In all cases, AE elicited only I_s responses in EGTA-loaded oocytes, while I_{osc} were eliminated, indicating that I_s was not Ca^{2+}-dependent, and confirming that I_{osc} was more probably activated through $[Ca^{2+}]_i$ increase. I_{osc} was the most robust response, whereas I_s showed lower amplitude, reaching values of 93 ± 83 nA (n = 22) (orange bar graph in Fig. 2c). No further analysis was performed on the mechanisms of I_{osc} activation. To explore the basic characteristics of I_s, its reversal potential (E_{rev}) was estimated in EGTA-loaded oocytes that were held at distinct membrane potentials while AE was superfused (Fig. 2d). I_s response had an E_{rev} close to − 20 mV in all cases

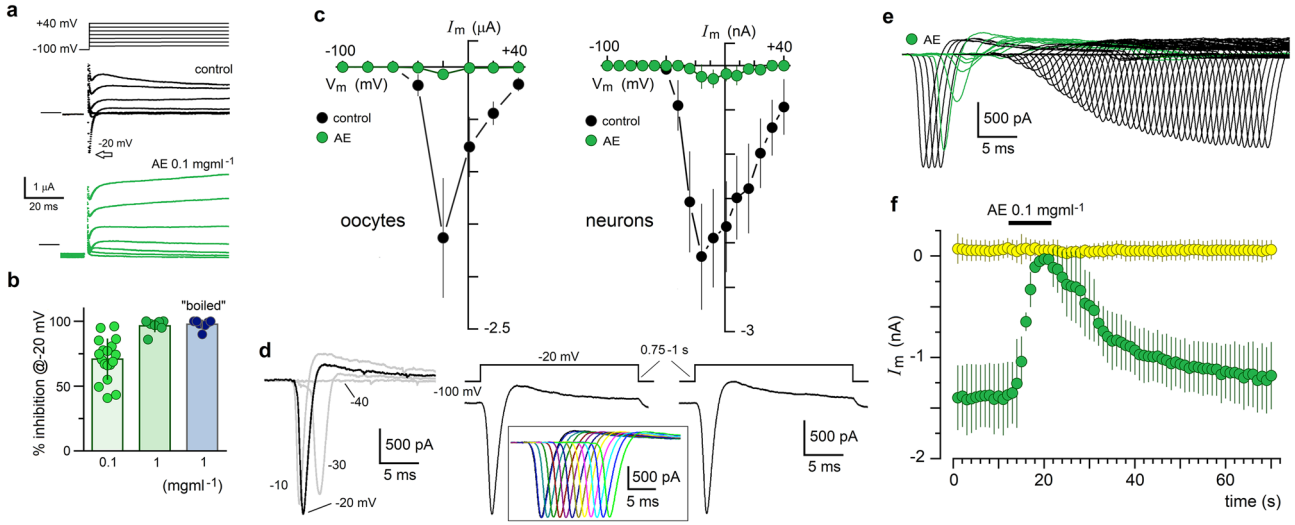

Figure 3. Anemone extract (AE) potently inhibited the I_{Nav} response in both mRNA-injected oocytes and in cultured cortical neurons. (**a**) Voltage-step protocol (from − 100 to + 40 mV) applied in mRNA-injected oocytes, held at − 100 mV, expressing voltage-dependent inward currents with a peak amplitude at − 20 mV, either in the absence (black traces) or the presence of AE (0.1 mg ml^{-1}; green traces). (**b**) Voltage-dependent inward current at − 20 mV was potently inhibited by AE in concentrations of 0.1 mg ml^{-1} (18 oocytes, 7 frogs) and 1 mg ml^{-1} (7 oocytes, 3 frogs), the inhibitory effect was not eliminated in samples "boiled" by 45 min (7 oocytes, 3 frogs). (**c**) I–V relationship for the inward current response in oocytes (left graph; n = 8) suggested that it corresponds to opening of Na_v channels; this was confirmed recording Na_v currents in cultured cortical neurons (right I/V graph, black circles, n = 5) that were also potently inhibited by 1 mg ml^{-1} superfusion (green circles); in both cases currents were inhibited in the whole voltage-range analyzed. (**d**) Traces illustrate the I_{Nav} activated in neurons at − 30, − 20 and − 10 mV from a holding potential of − 100 mV. Maximal currents were regularly obtained at − 20 mV, to test the effect of extracts in this and subsequent figures, I_{Nav} was elicited periodically, stepping the membrane potential from − 100 to − 20 mV for 20 ms every 0.75–1 s as illustrated in the traces on the right. To show the complete time-course of a particular experiment, traces were superimposed as this is shown in the insert that illustrates 12 consecutive stimuli. (**e**) In neurons, I_{Nav} current was activated periodically as in (**d**). After monitoring the control amplitude (black traces), neurons were exposed to 0.1 mg ml^{-1} AE (green traces) for 10 s. During AE application I_{Nav} was rapidly inhibited, and after this, AE removal allowed current recovery. The graph in (**f**) shows the effect monitored in 5 neurons (mean ± S.D.) using the protocol in (**e**), top black bar signals AE application; inward currents (green circles) were eliminated while small outward currents depicted in yellow circles showed no change.

tested (3 oocytes, 2 frogs). Also, Fig. 2e illustrates experiments where a protocol of pulses from − 100 to + 40 mV (in steps of 20 mV) was applied in the absence (control) and presence of AE. Thus, the I_s amplitude values elicited by AE in each potential were obtained by subtracting the corresponding control current values, and the results were plotted as illustrated. I_s presented an E_{rev} of − 22.7 ± 7.6 mV, like that obtained in Fig. 2d, suggesting a current mainly carried by Cl^- ions[36,39]. In the responses elicited by the pulse protocol, a fast voltage-dependent inward current that desensitizes within a few milliseconds was regularly activated (green circle in Fig. 2e; see also Supplementary Fig. S1). This current (denoted as I_{Nav}) corresponds with the opening of voltage-dependent Na^+ channels commonly expressed in brain mRNA-injected oocytes[40,41]. As depicted in Fig. 2e, I_{Nav} appears to be inhibited during the application of AE. Based on this initial screening, we decided to characterize in detail the AE effects on I_s activation and I_{Nav} inhibition.

Inhibition of I_{Nav}. AE was applied to mRNA-injected oocytes expressing I_{Nav} to quantify its effect within a potential range of − 100 mV to + 40 mV and explore its reproducibility in different preparations. The peak I_{Nav} amplitude at − 20 mV was inhibited 96.5 ± 4.97% by 1 mg ml^{-1} AE (7 oocytes, 3 frogs, Fig. 3a–c). However, the extract at 0.1 mg ml^{-1} still caused a potent inhibition of 70.8 ± 15.89% (18 oocytes, 7 frogs). AE samples boiled for 45 min fully maintained their inhibitory activity (7 oocytes, 3 frogs), indicating that the inhibitory substance was thermostable (Fig. 3b).

I_{Nav} kinetics monitored in the oocyte, within the entire range of potentials tested, results uncertain due to the oocyte size. Due to this, and to explore the effect of AE on endogenous molecules (i.e., I_{Nav} in neurons), the following experiments were performed using cultured rat cortical neurons. Figure 3c shows the I–V relationships for I_{Nav} generated either in mRNA-injected oocytes or in neurons, and for both cases in the absence (black circles) and the presence (green circles) of AE; it was found that inhibition by AE was similar in both preparations. Thus, I_{Nav} inhibition occurred in the entire range of membrane potentials and, importantly, AE had the same effect on neurons; for example, 0.1 mg ml^{-1} AE inhibited neuronal I_{Nav} by 95.3 ± 3% (5 cells). Figure 3d illustrates a typical example of neuronal I_{Nav} elicited by 20 ms voltage steps within the − 10 to − 40 mV range from a holding potential of − 100 mV, regularly, the maximum current amplitude was obtained at − 20 mV. To study the time-course of the

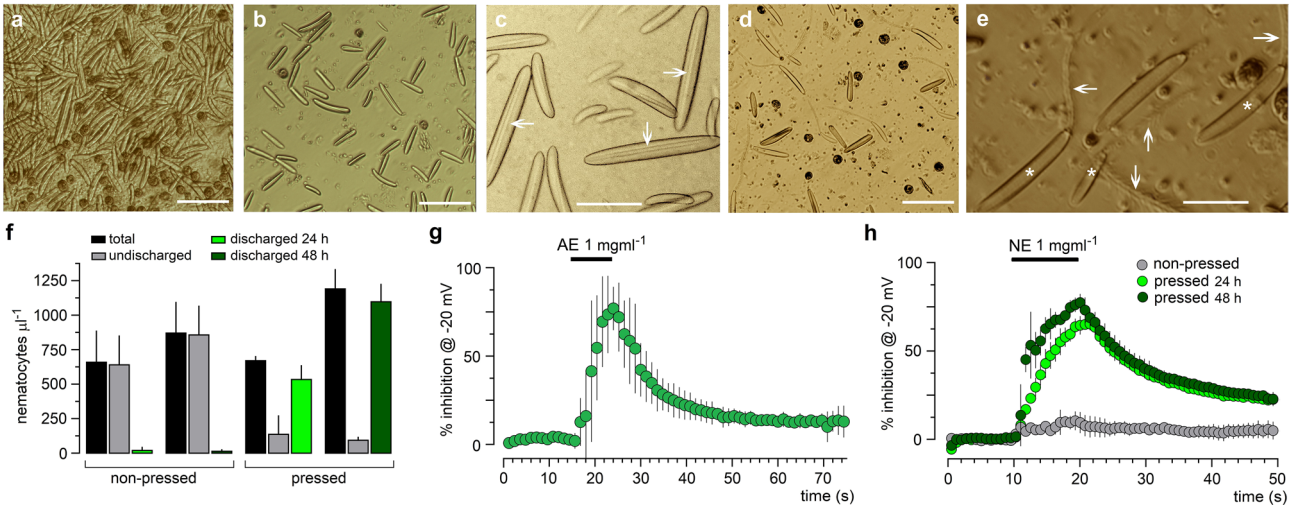

Figure 4. Nematocyst isolation and discharge using the French press cell disruption homogenizer. (**a**) Samples obtained from whole *B. annulata* anemone homogenate. (**b,c**) Samples recovered after 48 h following the Bloom's method showing mainly undischarged nematocysts. Arrows in (**c**) signal typical images of twisted tubules in the undischarged nematocysts lumen. (**d,e**) Samples as in (**b**) after being processed through the French press at 6.2×10^7 Pa, that provided mainly discharged nematocysts. Asterisks in (**e**) signal the nematocysts empty capsules and arrows indicate ejected tubules (bar = 50 µm in (**a,b,d**); bar = 20 µm in (**c,d**)). (**f**) Quantification of total (black columns), undischarged (gray columns), and discharged nematocysts (green columns) (per µl), for both non-pressed and pressed preparations in samples obtained by the Bloom's method either after 24 h (light green) or 48 h (dark green) (mean ± S.D.; *$p < 0.05$ for comparisons between pressed vs. non-pressed). (**g**) Typical effect of AE (1 mg ml^{-1}) on neuronal I_{Nav} response at − 20 mV (n = 6) using the same protocol as in Fig. 3. (**h**) A group of anemones from the same batch was processed by the Bloom's method and pressed either after 24 or 48 h, and the corresponding extracts were assayed on the neuronal I_{Nav} activated at − 20 mV (light and dark green, respectively). In gray is shown the lack of effect of the non-pressed 48 h sample. Individual data points in (**g,h**) represent the mean ± S.D. from 4 to 5 neurons.

effects of AE, and other treatments, pulses to − 20 mV were repeated every 0.75–1 s for several seconds (70–85 s; Fig. 3d) in such a way that the different treatments were applied for 5–10 s after a control period, followed by washing with external solution. The insert in 3d illustrates a series of control responses obtained using this protocol that have been superimposed to show I_{Nav} reproducibility, the time scale corresponds to that of a single depolarizing pulse. Typical results testing the effect of different treatments using this protocol were illustrated with superimposed traces as it is shown in Fig. 3e, where the time-course I_{Nav} inhibition by AE was analyzed by depolarizing the neurons from − 100 mV as described, after 10–12 voltage steps in control external solution (black traces) AE was superfused for 5–10 s (green traces) and the effect on I_{Nav} was monitored. Finally, AE was washed and I_{Nav} recovery followed for several seconds (traces in black). As this is shown in the bottom graph, application of 0.1 mg ml^{-1} of AE produced I_{Nav} inhibition with a τ_{50} of 2.88 ± 0.03 s (Fig. 3f, green circles; 5 neurons), while smaller outward currents activated at this potential were not significantly affected (yellow circles; most likely corresponding to voltage-gated K^+ channels). Recovery of inhibition required, in most cases, a 30–45 s wash. During I_{Nav} inhibition produced by AE, no change in the current inactivation rate was observed. For example, in a group of neurons (n = 6) the control time constant of inactivation was of 0.97 ± 0.48 ms, while after 3 s in the presence of AE (0.1 mg ml^{-1}), time in which more than 50% of I_{Nav} inhibition was regularly reached, this parameter was of 1.13 ± 0.7 ms. These values did not show a statistical difference.

All the experiments described above used AE, the homogenate of *B. annulata*. Although it is known that this method successfully discharges nematocysts, the venom obtained with AE clearly may include substances from other anemone tissues in addition to the nematocysts content per se (e.g. Ref.[20]) To confirm that effects were elicited by nematocysts content, a procedure for nematocysts isolation was done followed by controlled discharge through mechanical means. Figure 4a shows the sea anemone homogenate visualized using phase contrast microscopy. This sample contained a large number of nematocysts, together with symbionts and the sea anemone tissue itself. Comparatively, using a modified Bloom's method[42], and settling periods of 24–48 h (Fig. 4b) provided with nematocysts free samples of most of other animal tissue, also significantly reduced the number of symbionts. An amplification of these preparations showed the typical morphology of loaded nematocysts containing twisted tubules in their lumen (arrows, Fig. 4c). The purified nematocysts samples obtained after 24–48 h were then pressed to 6.2×10^7 Pascals using a French press. The extract obtained will be referred to as nematocysts extract (NE). The pressed preparations were then visualized under the microscope (Fig. 4d,e) to quantify the number of loaded and unloaded nematocysts after 24–48 h (Fig. 4f). Under the microscope, nematocyst discharge was visualized as an empty capsule associated with a large ejected tubule (asterisks and arrows, respectively in Fig. 4e). Figure 4f is a quantification made by triplicate of undischarged (gray bars) or discharged (green bars) nematocysts, in non-pressed aliquots compared with pressed aliquots from the same anemones

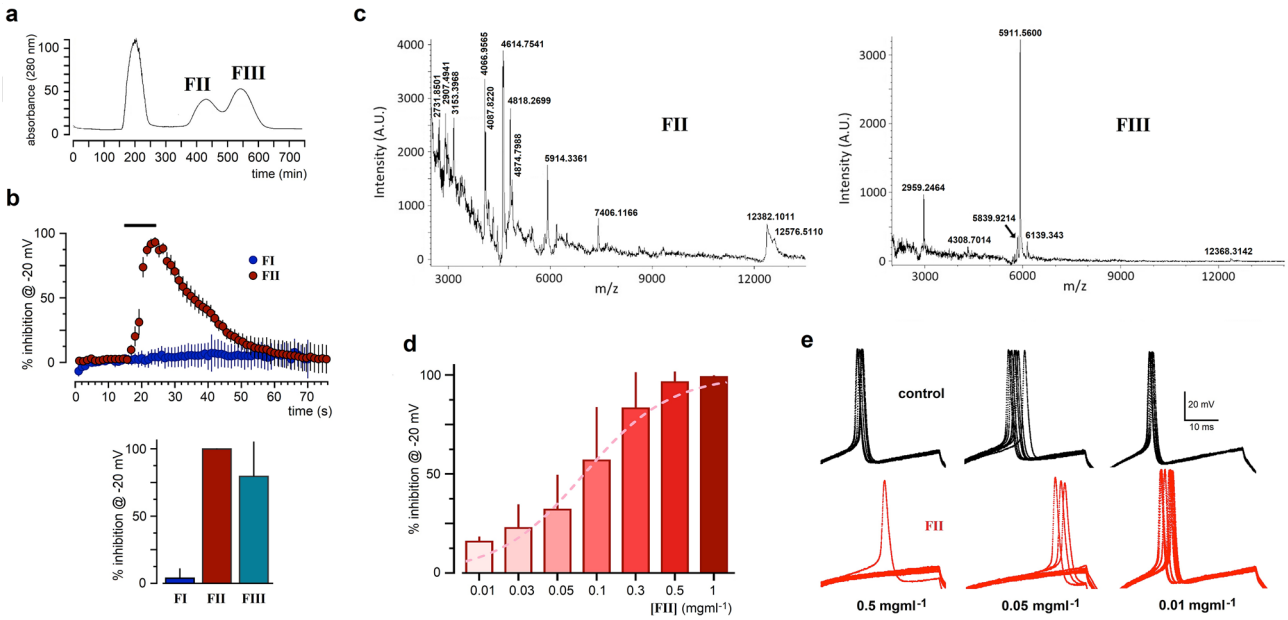

Figure 5. AE partial separation by Sephadex G-50 M chromatography, mass spectrometry, fraction dose-respond, and effect on the action potential. (**a**) Fractions obtained from AE gel filtration chromatography. Sephadex G-50 M column (90 × 8 cm) was equilibrated with PBS. Absorbance was monitored at 280 nm and fractions were collected at a flow rate of 300 µl min^{-1}. Three absorbance peaks were detected and the corresponding fractions (FI, FII, and FIII) were collected and tested for effect on neuronal I_{Nav} monitored at − 20 mV (6–14 neurons in each case, held at − 100 mV and depolarized every 750 s for 20 ms). (**b**) The graph shows I_{Nav} inhibition time-course produced by FII (1 mg ml^{-1}; 11 neurons), while FI did not produce a significant effect (4 neurons; mean ± S.D.), the column graph resumes the inhibition produced by each fraction (1 mg ml^{-1}). (**c**) MALDI-TOF–MS spectrum obtained from the FII and FIII fractions obtained from AE gel filtration chromatography, the numbers indicated the mass for the main signals detected. In (**d**) FII was applied in distinct concentrations and a dose–response curve (in pink) was adjusted to data points indicating an EC_{50} of 80 ± 16 µg ml^{-1}. (**e**) FII was tested on the neuronal action potential generated by depolarizing steps (35 ms, 0.75 nA) every 500 ms; three decreasing FII concentrations are illustrated. Traces in black (10 superimposed traces in each case) corresponded to control action potentials before FII superfusion, whereas red traces were obtained during FII application. 0.5 mg ml^{-1} potently inhibited the action potential, a concentration 10 times lower still blocked completely the action potential in few seconds, while 0.01 mg ml^{-1} FII was ineffective.

samples. Quantification showed that in both 24-h and 48-h groups the efficiency of total nematocysts recovery increased, and that a small proportion of non-pressed nematocysts were already discharged. More importantly, it revealed that pressing led to a significant nematocysts discharge. For instance, from a total of 1190 ± 144 nematocysts per µl after 48 h of incubation, the pressed sample rendered 1096 ± 130 discharged nematocysts per µl; thus, most nematocysts were discharged after being pressed.

The time-course and potency of the effect for both AE and NE on neuronal I_{Nav}, using the protocol as in Fig. 3d–f, is shown in Fig. 4g,h. First, 1 mg ml^{-1} AE inhibited I_{Nav} by 77.9 ± 12.6%, while NE (1 mg ml^{-1}) obtained from the same anemones batch, incubated for 24 or 48 h, inhibited I_{Nav} by 56.8 ± 5.2% (light green circles) and 69.4 ± 4.4% (dark green circles), respectively (Fig. 4h). Both NE samples showed lower inhibition amplitude with a slower time-course compared to AE; however, the inhibitory effect was similar. The 48-h non-pressed (gray circles) sample presented low activity on I_{Nav} (peak inhibition of 9.2 ± 4.7%). Altogether, these data strongly suggested that the effect on I_{Nav} was due to a substance or substances contained in the nematocysts of *B. annulata*.

As a first approach for separation and purification of the toxins responsible for the effects, chromatography was performed with a Sephadex G-50 M column that allows substances separation based on their molecular weight. Chromatographic pattern from AE separated three peaks that were identified as FI, FII and FIII fractions (Fig. 5a). The bioassay of these fractions (Fig. 5b) on neuronal I_{Nav} indicated that 1 mg ml^{-1} FI did not affect I_{Nav}, while FII was a potent fraction reaching inhibition values of 99.82 ± 0.47%. FIII also showed activity reaching an inhibition of 79.5 ± 25.9%, although its effect exhibited greater dispersion. The inhibitory time-course by FII was like that observed with AE and NE (Fig. 5b).

Since FII and FIII elicited I_{Nav} inhibition, a chemical analysis using MALDI-TOF mass spectrometry was done as this is shown in Fig. 5c. Both fractions showed peptides with molecular masses between 3 and 12 kDa, however, FII was more complex in composition than FIII. Importantly, the molecular masses observed were in the range of those reported for sea anemone neurotoxins (3–7 kDa)[6]. The presence of apparently equivalent components, in FII (e.g., m/z 5914.34 and 12,382.10) and FIII (m/z 5911.56 and 12,368.31) (Fig. 5c), might be an explanation for similar effects in both fractions.

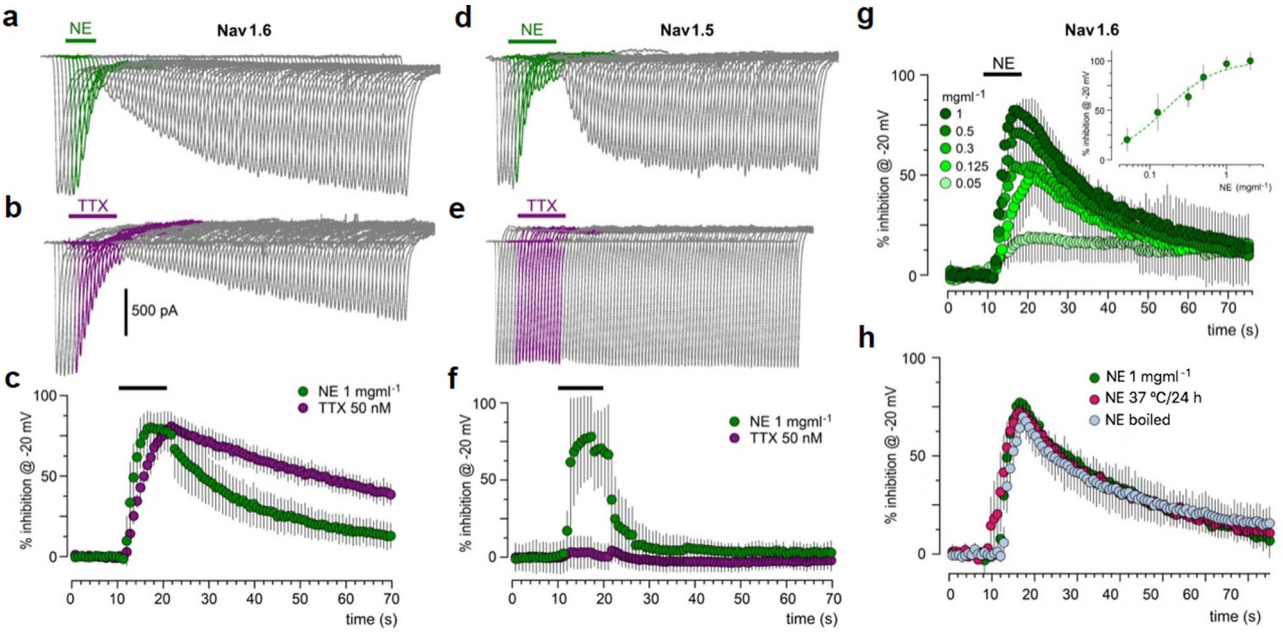

Figure 6. Nematocysts extract (NE) from *B. annulata* potently inhibited I_{Nav} elicited by opening of $hNa_v1.6$ and $hNa_v1.5$. (**a**) HEK293 cells expressing $hNa_v1.6$ channels were recorded and I_{Nav} was activated applying voltage steps from − 100 to − 20 mV, using a similar protocol to that used in Fig. 3c. In the experiment illustrated, 1 mg ml^{-1} NE was applied as indicated by the bar in green after a control recording of I_{Nav} (traces in gray); during NE superfusion I_{Nav} decreased progressively (traces in green) and recovered during wash. (**b**) Traces show the effect of 50 nM TTX (purple traces) using the same protocol in cells from the same cultures. The graph in (**c**) shows the time-course of the inhibitory effect produced by each treatment (mean ± S.D. from 6 to 10 cells). (**d,e**) HEK293 cells expressing $hNa_v1.5$ channels were recorded in similar manner and tested for either NE (traces in green) or TTX (traces in purple); as expected TTX did not affect I_{Nav}, but NE strongly inhibited the response. The inhibition time-course produced by NE is illustrated in (**f**) together with the lack of effect by TTX; individual data points are the mean ± S.D. (5 cells in each case). (**g**) A dose–response relationship was built for the NE effect on the I_{Nav} in cells expressing $hNa_v1.6$ channels (top graph); distinct NE concentrations from 1 to 0.05 mg ml^{-1} were applied to 6 different cells. Individual data points are the mean ± S.D. of the effect. Then, the normalized peak inhibition for each concentration was plotted (insert graph) and data points were fitted to a dose–response curve (green dashed line, $EC_{50} = 155 \pm 34$ µg ml^{-1}). (**h**) The graph shows the time-course of I_{Nav} inhibition produced by 1 mg ml^{-1} NE (green circles), and the effect produced by NE from the same batch that was boiled by 15 min (light blue circles) or NE samples that were incubated at 37 °C overnight (pink circles); individual data points are the mean ± S.D. from 5 cells in each case.

The sensitivity of I_{Nav} to FII clearly presented a dose–response (D-R) relationship with a mean dose of 80.4 ± 16 µg ml^{-1} (Fig. 5d). Also, FII was used to analyze in cultured neurons its effect on action potential generation. For this, constant current pulses (0–65-0.85 nA) were applied to generate action potentials every 1–1.2 s at 30% above threshold amplitude, to avoid failures in impulse generation. Then, different solutions containing 10 µg to 1 mg of FII were applied for 10 s (n = 4, Fig. 5e). Complete action potential inhibition was observed in a dilution as low as 0.05 mg ml^{-1} after 3–4 s of superfusion, while a robust inhibition effectiveness was observed from 0.1 to 1 mg ml^{-1}. FII produced a fast action potential blockage, and the duration was not affected during FII application. At all concentrations tested, the recovery of action potential amplitude was complete after washing.

Tetrodotoxin (TTX) is a potent Na_v channel blocker[43], the molecular identity of the TTX binding site on the channel is well known[44]. To know whether NE inhibition effect was produced acting on the same or similar TTX binding site, extract was tested in HEK293 cells expressing either $hNa_v1.6$ or $hNa_v1.5$ channels. As it is well known, TTX acts differentially on distinct I_{Nav} subtypes; $hNa_v1.6$ is a TTX-sensitive channel, whereas $hNa_v1.5$ is essentially a TTX-insensitive channel[45]. I_{Nav} currents in HEK cells were recorded similarly to those in neurons; thus, current responses were activated by depolarizing the cell periodically to values around the peak current. As is illustrated in Fig. 6a,c, 1 mg ml^{-1} NE superfusion inhibited the current elicited by $hNa_v1.6$ opening as strongly as the blockage produced by 50 nM TTX (Fig. 6b,c). Remarkably, 1 mg ml^{-1} NE also strongly inhibited the current generated by $hNa_v1.5$ channel activation (Fig. 6d,f). As expected, in these same cells the I_{Nav} current was not blocked by TTX (Fig. 6e,f). Also, comparing the rates of inhibition and recovery of NE and TTX on the $hNa_v1.6$ current, NE seemed to act faster than TTX, and 155 ± 34 µg ml^{-1} NE inhibited 50% of I_{Nav} (Fig. 6g). Like that observed with AE, NE (1 mg ml^{-1}) either boiled for 15 min or incubated for 24 h at 37 °C, fully retained activity (Fig. 6h).

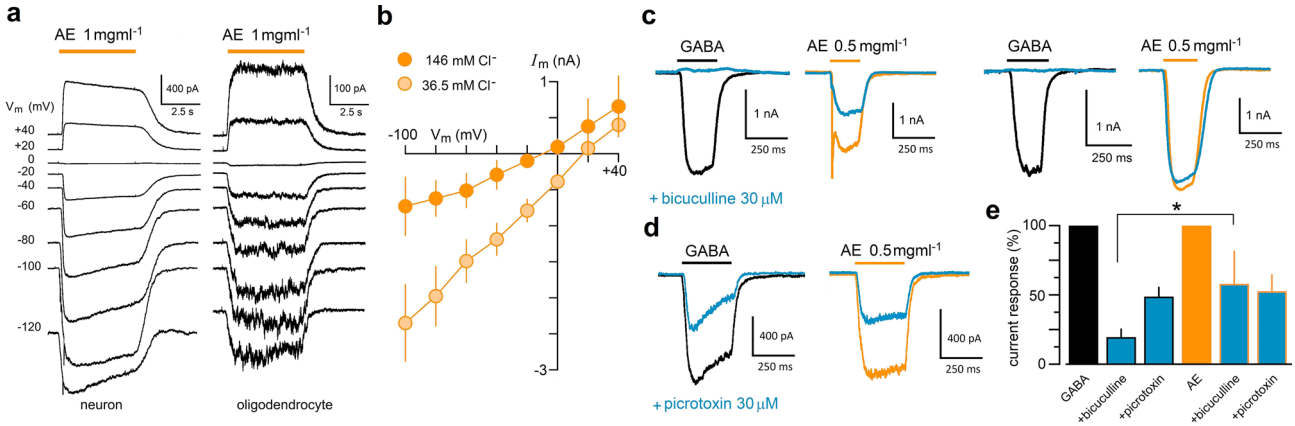

Figure 7. Ionic basis and pharmacology of inward currents generated by AE in neural cells. (**a**) Traces illustrate typical current response elicited by AE (1 mg ml^{-1}) at different potentials either in neurons or in oligodendrocytes; in both cases extract generated inward currents that presented an E_{rev} close to 0 mV. (**b**) Current–voltage relationship for the response to AE were monitored in neurons in two conditions, first in control external solution containing 146 mM Cl^- (dark orange circles) and then the same cell in external solution containing 36.5 mM Cl^- (light orange circles). In low Cl^- external solution the E_{rev} shifted to more positive potentials. (**c**) Bicuculline (30 μM) was tested for its effect on the inward current response elicited by AE (0.5 mg ml^{-1}). Neurons were tested for their response either to 5 μM GABA (black traces) or to AE (orange traces) and then the inhibitory effect of bicuculline (blue traces) was tested in each case. For GABA response bicuculline showed a strong inhibitory effect in all cases, while the effect on AE-elicited response was less potent and more variable between different neurons (two different neurons are illustrated). (**d**) In similar experiments, picrotoxin (30 μM, blue traces), inhibited in comparable manner to both the GABA- and the AE-response. (**e**) Normalized responses (mean ± S.D.) obtained in 8 neurons for each condition are shown in the bar graph. Current response in the presence of each drug was normalized against the corresponding amplitude reached by either GABA or AE applied alone (*$p < 0.05$ for comparisons between the GABA vs. AE amplitude values in the presence of bicuculline).

Generation of I_s response and $GABA_A$ receptor activation. AE consistently generated a smooth inward current (I_s) associated with an increase in membrane conductance in mRNA-injected oocytes (Fig. 2b–e). This response was generated in both neurons and oligodendrocytes, although the amplitude response was clearly weaker in the latter cell type, as illustrated in Fig. 7a. In oocytes, the estimated E_{rev} corresponded with the flux of Cl^-; thus, the I–V relationship for the inward response was built for neurons (Fig. 7b). We also found that the E_{rev} for the inward current response in external solution containing 146 mM Cl^- was of − 8.8 ± 3.5 mV, while in solution with reduced Cl^- concentration (36.5 mM) the E_{rev} shifted to a potential of + 16.2 ± 4.3 mV, and the inward current amplitude became larger; altogether, these results suggest that inward current response was mainly carried by Cl^-. The main Cl^- channel in neurons is $GABA_AR$. To explore a possible $GABA_AR$ involvement in the response elicited by AE, the extract was coapplied in neurons with either 30 μM bicuculline or picrotoxin, an antagonist and a blocker of the $GABA_AR$, respectively. In neurons (Fig. 7c–e; 5–7 neurons), bicuculline inhibited to 19 ± 18.1% the current elicited by 30 μM GABA, whereas picrotoxin blocked around 50% of the GABA response (to 48.2 ± 7.6%). In the same neurons, bicuculline and picrotoxin inhibited the current activated by 0.5 mg ml^{-1} AE to 57.5 ± 24.4% and 52.2 ± 12.8%, respectively (Fig. 7e). Contrary to what was observed in the GABA-generated current, bicuculline had a more variable effect on the inward current elicited by AE (see Fig. 7c), although picrotoxin presented a similar blocking effect either with GABA or AE stimulation (Fig. 7d).

The FI-FIII fractions obtained by chromatography also showed differential potency on neurons, thus 1 mg ml^{-1} FI was ineffective (7 neurons) to generate the inward response, 1 mg ml^{-1} FII generated inward responses of 1128 + 763 nA (13 cells), while FIII generated weak responses of 170.3 + 112 nA (7 cells), suggesting that the effect was elicited for a substance mainly contained in fraction FII.

To confirm a direct action on $GABA_AR$ by AE and NE, receptors were expressed in oocytes. Expression of the most common neuronal $GABA_AR$, comprised by α1β2γ2 subunits, provides sensitivity to GABA superfusion (Fig. 8a). Oocytes responding to 10 μM GABA were also sensitive to 0.5 mg ml^{-1} AE superfusion, generating smooth inward currents that opened rapidly after beginning the application and stayed activated until GABA or AE were washed out. To make the application of AE more efficient, the extract was applied through a jet of solution ejected close to the oocyte surface. Extract solution jet application was a reproducible method of stimulation that consumed minimal amount of venom (Fig. 8a). The AE jet application method did not generate any response in native oocytes (Fig. 8b); however, in oocytes expressing the neuronal $GABA_AR$, the delivery of either AE or NE prompted a rapid inward response that, as expected, had an E_{rev} of − 22.8 ± 2.6 mV (Fig. 8c). $GABA_ARs$ composed of other subunits expressed in oocytes were also activated by AE and by NE applied in similar manner; thus, receptors comprised by α3β2γ1 subunits typically expressed in oligodendroglial cells[46] and homomeric ρ1 GAB_AR[47] were also operated by the extracts. The α3β2γ1 receptor has an EC_{50} for GABA of 80 μM, with a threshold for the response close to 1 μM (Fig. 8d, red traces). The typical neuronal receptor expressed in

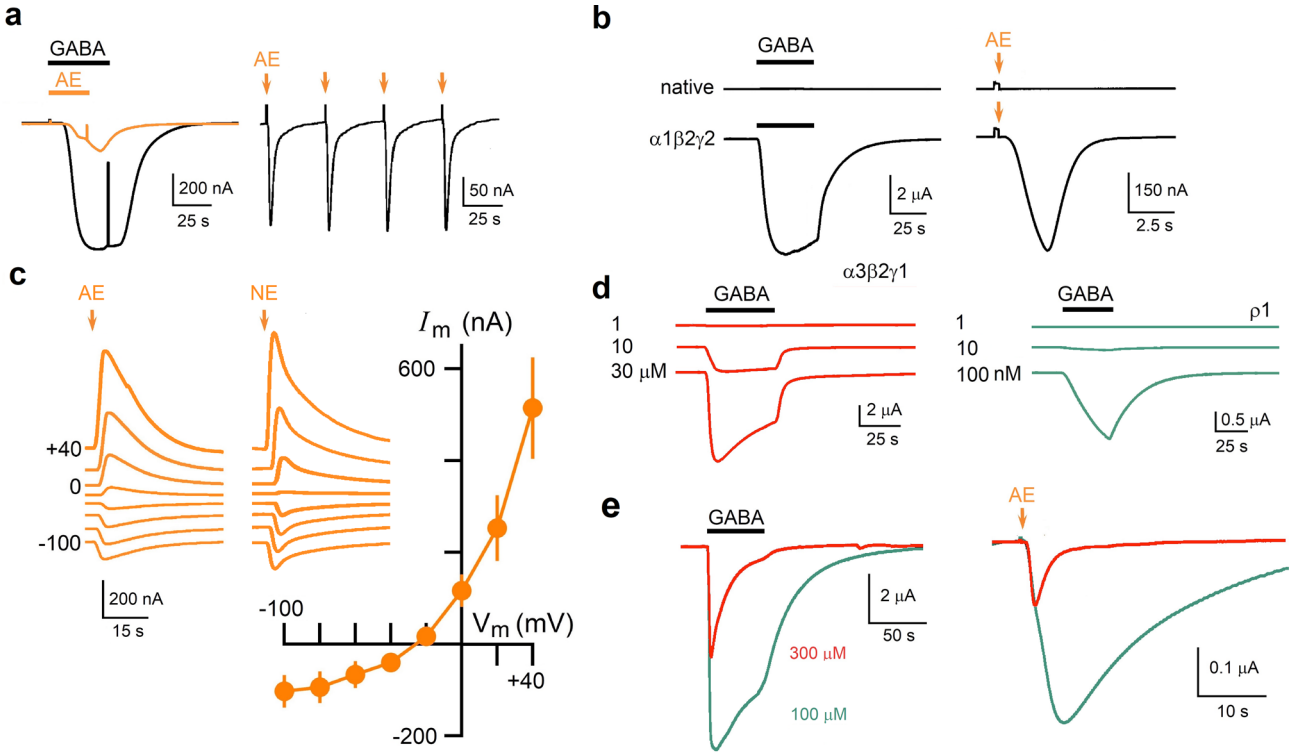

Figure 8. *B. annulata* venom contains an agonist of $GABA_A$ receptors. (**a**) Traces on the left illustrate inward current responses in *Xenopus* oocytes expressing the neuronal $GABA_A$ (α1β2γ2) receptor; cells were held at − 60 mV and superfused with either GABA (10 μM; black trace) or AE (1 mg ml^{-1}; orange trace). In the trace on the right, AE was applied close to the oocyte surface using the jet delivery method, which consists of a small volume (25–75 nl) ejected from a micropipette filled with solution containing AE (0.5 mg ml^{-1}), four AE-jets (orange arrows) applied successively show that current responses generated were robust and reproducible. (**b**) Top traces show that native oocytes (H_2O-injected) were not sensitive to GABA superfusion or to AE jet-delivery (orange arrow indicates jet activation), while oocytes from the same frog expressing the neuronal $GABA_A$ receptor (bottom traces) generated robust current responses to both GABA and AE. (**c**) Traces are responses at different holding potentials from − 100 to + 40 mV elicited either by jets of AE or NE as indicated; the graph is the current–voltage relationship of the responses by AE applying the same protocol in 6 different oocytes (2 frogs); individual data points are the mean ± S.D. of the peak current response in each potential. (**d,e**) AE (and NE) affects two more $GABA_A$ receptor types expressed in oocytes, the oligodendroglial receptor α3β2γ1 (red traces) and the homomeric ρ1 receptor (green traces). Traces in (**d**) show the current response to GABA around the concentration threshold for each receptor, 1 μM for α3β2γ1 and 10 nM for the ρ1 receptor. In (**e**) the traces on the left illustrate responses elicited by a maximal concentration of GABA in oocytes expressing the α3β2γ1 receptor (in red) or the ρ1 receptor (trace in green), while the traces to the right show the response in the respective oocytes elicited by the same dose of AE. Traces are representative of results obtained in 7 oocytes from 3 different frogs.

the oocyte membrane has an EC_{50} around 100 μM with a threshold also close to 1 μM, while the homomeric $GABA_AR$ ρ1 has an EC_{50} of 1.2 μM, with a threshold within the nanomolar range (Fig. 8d, green traces). Using the same conditions and micropipette for jet application, responses to AE had an expected amplitude for the respective GABAAR expressed; thus, α3β2γ1-receptor responses were lower in amplitude, while ρ1-receptor responses were consistently larger (Fig. 8e).

These results suggested that extracts could contain GABA at a concentration within the micromolar range; thus, AE samples were analyzed using a GABA-specific ELISA test (with nanomolar detection sensitivity). However, AE and NE samples (3 different extracts) that activated robust responses in oocytes expressing either the α1β2γ2- or the α3β2γ1-receptor reported a GABA concentration of 9.97 ± 1.8 nM in the ELISA test, which by itself did not explain the observed amplitude responses. This strongly suggested that *B. annulata* venom contained a potent $GABA_AR$ agonist different to GABA.

Discussion

More than sixty toxins affecting Na_v channels have been isolated from sea anemones, most of them cause a delay in Na_v channel inactivation[48,49]. The results described here show two novel toxic effects exerted by substances contained in the nematocysts of the sea anemone *B. annulata*, each one acting on fundamental membrane proteins of the mammalian nervous system: the Na_v channel and the $GABA_AR$. The recognition of species of interest, due to specific effects of their toxins and/or by their venom potency, is undoubtedly an advantage to

direct the search for new bioactive principles. Here we show that *B. annulata* venom contains substances that act on the nervous system of both vertebrates and invertebrates, as seen by the effects on crabs and on membrane proteins of vertebrates, specifically those from the nervous system of mammals (including human). The novelty of the effects described here, clearly indicates the importance of studying the potential bioactivity of cnidarian families that remain unexplored.

In several experiments of this study, nematocysts of *B. annulata* were first isolated using a modified Bloom's method[42], and then subsequently discharged in a controlled manner, applying pressure conditions that did not affect the symbiont structural integrity, as previously reported[50]. This increased the certainty that the effects observed were generated by compounds contained in the nematocysts, since extracts that were not pressed had reduced activity compatible with the basal discharge observed by nematocysts quantification.

Na_v and $GABA_AR$ channels are crucial in neural functions and effects on them could explain by themselves the venom lethality[30,51,52]. Na_v channels are responsible for nerve impulse generation, while $GABA_ARs$ are important effector molecules of GABA, the main inhibitory neurotransmitter in the nervous system. Until now, most neurotoxins isolated from sea anemones (e.g., ShK, BgK, CgNa, and CGTX II) affect K_v or Na_v channels[13,53–59]. The peptide neurotoxins that act on Na_v channels are widely studied and have been classified into four types[6]. It is known that the action mechanism of many toxins from anemones involves their binding to open Na_v channels, causing a delay in channel inactivation and an increase in action potential duration[57,60,61]. However, different to this mechanism, our results showed that *B. annulata* venom contains a substance that inhibits the Na_v current response at the whole voltage range tested, without affecting both the inactivation rate, and apparently neither the voltage dependency of activation. Also, I_{Nav} inhibition more probably caused a rapid and dose-dependent blockage of the action potential generation in cortical neurons with no effect on its duration, suggesting that the inhibitory effect of *B. annulata* venom was more compatible with a blockage of the Na_v channel pore, although a complete definition of the inhibition mechanisms involved will require of further experiments. The chemical identity of the toxin(s) remains to be elucidated; however, it would correspond to a heat-stable molecule of more than 3000 Da. These features agree with the results of mass spectrometry analyses of FII and FIII that showed the presence of peptides in the expected range. Thermostability of anemone toxins has been reported in several cases and, this characteristic has been associated with the stability provided by the presence of disulfide bridges in its structure (e.g., Refs.[6,51,62]). It is also evident that its action mechanism was not identical to that of TTX, because *B. annulata* venom inhibited both the human $Na_v1.6$ and $Na_v1.5$ channel current responses, which clearly differ in their sensitivity to TTX[45,63]. It is still possible that *B. annulata* bioactive substance, described here, shares an overlapping binding site with TTX, and some small change in Nav1.5 is enough to interfere with TTX and not with that of *B. annulata*.

A different binding site for pore blockage in Na_v channels is that of the cone snail toxin GIIIA[64], more experiments will be necessary to establish its possible participation in the *B. annulata* venom effect. The functional study of new molecules that affect Na_v channels in mammals remains limited. Hence, the discovery of new template molecules that could act in a more specific and differential manner is of general interest for the design and development of novel molecular tools (e.g. Ref.[65]). Furthermore, Na_v channels regulation are important not only for nervous system physiology but also because of their possible role in various diseases including cancer[66–69].

A second molecule in the venom, acting as a GABAergic agonist, also represents a new action mechanism for sea anemone toxins, and its rapid action opening the channel in the millisecond range, as well as the complete recovery upon wash, resembles the action of the full agonist muscimol produced by the fungus *Amanita muscaria*[70]. Several natural substances act on $GABA_AR$ and many are drugs that have powerful effects on the nervous system (e.g., picrotoxine, β-carbolines). Also, peptides that inhibit $GABA_ARs$ have been previously described in marine animal venoms in at least two species, *Laticauda semifasciata* and *Conus imperialis*[71]. In the case of *B. annulata* venom, the active substance operated three $GABA_AR$ types with different molecular identities (either neuronal or glial heteromeric receptors, as well as the ρ1 homomeric receptor); thus, this suggested that the venom contained concentrations in tens of the micromolar range of GABA. The expression of the GABAergic signaling system has been documented in cnidarians where it has been related to nematocyst discharge regulation, among other functions[72]. However, results of ELISA assays with sensitivity to nanomolar GABA concentration showed that the venom contained GABA in around 10 nM. This indicated that the molecule responsible for $GABA_AR$ activation was of a different nature since this concentration was too low to activate either the neuronal or the oligodendroglial receptor. Alternatively, the venom could contain a potent positive modulator that would increase the $GABA_AR$ sensitivity to GABA.

Nevertheless, our results also suggested that $GABA_ARs$ were not the only receptors activated by the venom. Thus, testing the venom on cortical neurons revealed that currents produced in some cells, persisted even after its co-application with bicuculline, a potent competitive antagonist of the GABA site. This finding could also be explained by a different competition mechanism between bicuculline with the active substance as compared with GABA. On the other hand, the importance of a molecule in the venom that depresses the activity of the central nervous system seems to be clear, and it is striking that this mechanism apparently is not common among the venoms studied so far, since combining it with a powerful Na_v channel blocker molecule would result in a fast-acting bioweapon.

The advancement of robust biochemical and molecular techniques will provide detailed information about the identity of substances contained in the venom of many species that remain unexplored, including cnidarians. This study showed that the common Caribbean *B. annulata* is a source of novel neurotoxins that potently target essential proteins for the functioning of the mammalian central nervous system.

Conclusion

The number of marine species that synthesize bioactive molecules studied is far from being exhausted, these molecules are widely diverse, and their molecular targets are of great interest in terms of basic mechanisms and for the development of new therapeutic and experimental tools. The use of heterologous expression models for the recognition of target molecules, such as the expression in *X. laevis* oocytes, represents a useful method to recognize relevant effects of the venoms. Here, oocytes expressing mammalian brain ion channels and membrane receptors revealed effects of the *B. annulata* venom on two of the most important proteins for the functioning of the nervous system, Na_v channels and $GABA_A$Rs.

Materials and methods

Animal ethics declarations. All animal studies complied with the ARRIVE guidelines. All the animals were treated with the utmost care to minimize their suffering and were handled in accordance with the *Guide for the Care and Use of Laboratory Animals* by the USA National Institutes of Health, as well as the Local Guidelines on the Ethical Use of Animals for Experimentation at the Universidad Nacional Autónoma de México. *B. annulata* sample collection was carried out through permit no. PPF-066/20 from Dirección General de Ordenación Pesquera y Acuicultura, Quintana Roo, México.

Sea anemone collection and venom extraction. Specimens of *Bartholomea annulata* were collected from the reef lagoon at Puerto Morelos, Quintana Roo, México (20° 50′ 45″ N 86° 52′ 08″ W; 20° 50′ 55″ N 86° 52′ 52″ W) by SCUBA diving (Fig. 1).

The venom extracts were prepared using two different methods, as follows: (1) *Sea anemone macerate to obtain* AE was carried out as described elsewhere[29]. Briefly, whole sea anemone bodies were homogenized in deionized water to perform the nematocysts discharge. Rupture of nematocysts was monitored by microscopy until most nematocysts were discharged. The extract obtained was centrifuged at $3.2 \times 10^3 \times g$ at 4 °C for 10 min, the supernatant was decanted, and the same procedure was applied one more time. Finally, the supernatant was dialyzed using a pore size limit of 3000 Da, lyophilized and frozen until it was used. (2) *Nematocyst's isolation and discharge* to obtain NE. To avoid contamination of the extract with other cells or tissues, sea anemones were washed with filtered (0.45 µm) sea water to remove sand and small stones[57], then they were exposed to six freeze–thaw cycles. Sea anemone bodies were immersed in two volumes of distilled water kept at 4 °C and stirring every 10 min for 2 h (modified from Ref.[42]). Samples were filtered with a 100-µm-mesh and the filtered material was allowed to settle for either 24 h or 48 h. After the settlement period the sediment was washed three times, first with phosphate buffer solution (PBS, containing in mM: 2.74 NaH_2PO_4, 7.2 dibasic Na_2HPO_4) plus 0.01% Triton, and then twice with PBS alone. The precipitate was visualized under a microscope to monitor the number of undischarged nematocysts. Then, discharge of these organelles was carried out applying a pressure of 6.2×10^7 Pa using a French press cell disruption homogenizer (SLM-AMINCO, Urbana, IL, USA). It has been reported that symbionts are affected applying a higher pressure of 8.3×10^7 Pa[50]. Finally, samples were centrifuged at 10^5 g for 1 h at 4 °C, and the supernatant containing the venom was dialyzed using a pore size limit of 3000 Da, lyophilized, and kept at − 30 °C.

Toxicity test. Both extracts were tested in *Ocypode quadrata* crabs, collected from the Puerto Morelos beach. Aliquots (50 µl) of either extract dissolved in PBS, or PBS alone as a control, were injected through the third walking leg[29,33].

Size exclusion chromatography. The AE was fractionated using Sephadex G-50 M. The column was equilibrated with PBS. Samples dissolved in the same buffer were eluted to a flow rate of 300 µl min^{-1}, with monitoring at 280 nm, and 5-ml fractions were collected. The fractions were concentrated with reduced pressure ("rotary evaporator"), dialyzed using a pore size limit of 3000 Da, and lyophilized.

Mass spectrometry. Fractions FII and FIII were chemically analyzed using MALDI-TOF mass spectrometry. 5 µl of a saturated solution of sinapinic acid (> 99.0% purity for MALDI-MS, Sigma, St. Louis, MO, USA) were added to 5 µg of lyophilized of each fraction. 1 µl of this solution was deposited onto the MALDI plate and allowed to dry at room temperature. The spectrum was recorded on linear positive mode on a mass spectrometer (Microflex Bruker Daltonics, Bremen, Germany) equipped with nitrogen laser λ = 337 nm and a 20 kV acceleration voltage.

mRNA and cDNA. The poly(A)-mRNA was purified from adult Wistar rat brains; for this, mRNA was extracted from the whole brain using the guanidinium/phenol/chloroform method followed by oligo(dT)-cellulose chromatography[73]. The mRNA pool used here was purified from 19 different extractions from the same number of brains, each extraction was analyzed for its quality by electrophoresis and the ratio of absorbance 260/280 nm, as well as for its expression capacity of ion channels and membrane receptors into oocytes from different frogs. It was dissolved to 1 ng nl^{-1} in water and stored at − 80 °C until its use for expression using *Xenopus* oocytes.

The cDNA coding sequences for α1, α3, β2, γ1, and γ2 subunits of the $GABA_A$R were obtained as previously reported[46] from neural tissue, while ρ1 subunit coding sequence was donated by Dr. Ataúlfo Martínez-Torres[47]. All subunits were amplified, and each fragment obtained was cloned into pXENEX1 vector at the Ncol, BamHI, and NotI sites, then plasmids were linearized with the Hind III enzyme and used as templates for cRNA in vitro synthesis using the T7 mMESSAGE mMACHINE kit following the standard protocol (Ambion Invitrogen,

Grand Island, NY, USA). cRNA was dissolved to 0.1 ng nl^{-1} in water and used for heterologous expression in *Xenopus laevis* oocytes.

Heterologous expression in *Xenopus* oocytes and electrophysiology. Oocytes at stages V and VI[74] were dissected from ovary lobules of *Xenopus laevis* and microinjected either with 50 nl of mRNA (1 ng nl^{-1}) purified from rat brain or 50 nl of solution containing $GABA_A$ cRNA (5 ng per oocyte)[75]. After 48 h, the injected oocytes were treated with collagenase (0.5 mg ml^{-1}) at room temperature for 30 min in normal frog Ringer's (NR) solution (containing in mM: 115 NaCl, 2 KCl, 1.8 $CaCl_2$, 5 HEPES, pH 7.0)[15]. Finally, oocytes were kept at 16–18 °C in sterile normal Barth´s solution (containing in mM: 88 NaCl, 1 KCl, 2.4 $NaHCO_3$, 0.33 Ca $(NO_3)_2$, 0.4 $CaCl_2$, 0.82 $MgSO_4$, 5 HEPES, supplemented with 70 µg ml^{-1} gentamycin, pH 7.4) until they were used for electrical recordings.

Two or more days after injection, the membrane currents were recorded using the two- electrode voltage-clamp technique[38]. Microelectrodes (1 MΩ) were inserted into the oocyte and transmembrane currents were monitored using an Axon GenClamp 500 B (Molecular Devices, San Jose, CA, USA) amplifier. Signals were digitized and stored using an analog-to-digital convertor (Axon DigiData 1200; Molecular Devices) and specialized software (pClamp v9; Molecular Devices)[75].

Unless otherwise stated, oocytes were held at − 60 mV and continuously superfused (10 ml min^{-1}) with NR. The venom and distinct neurotransmitters (serotonin, 5 HT; γ-aminobutyric acid, GABA; acetylcholine; glutamic acid) were applied regularly by superfusion. To activate voltage-dependent ionic channels, mainly Na_v channels, a protocol of voltage steps was applied to build the current–voltage (I–V) relationships. Voltage-step protocols were applied while oocytes were held at − 100 mV and membrane potential was changed from − 80 to + 40 mV in steps of 20 mV for 250 ms, current responses were measured either at the steady-state or at the peak of the inward current, for I_s response or I_{Nav}, respectively.

Injection of 500 pmol ethylene glycol-bis(β-aminoethylether)*N*,*N*,*N*′,*N*′,-tetraacetic acid (EGTA) into oocytes was made by pneumatic pressure ejection from micropipettes containing 200 mM EGTA solution (plus 5 mM HEPES, adjusted to pH 7.0 with KOH)[38].

The method of drug application by superfusion regularly requires of a high sample volume (10 ml per min of application) for oocyte recording. Here, a much more efficient delivery system for the extracts was used (Fig. 8). This method consisted of applying the extract sample, either AE or NE (in NR solution), through jets of solution from a micropipette placed near the surface of the oocyte (approximately 100 µm), while maintaining the general flow of the external medium at a minimum level of 0.5 ml min^{-1}; then the extract contained in the micropipette was ejected by applying small pulses of pressure through the opposite end. The pressure (regularly 10–20 PSI) was controlled through a manometer as well as by modifying the pulse duration. In this manner small volumes of test solution were applied. Regularly jets of few nanoliters (25–100 nl) were enough to activate current responses in oocytes expressing $GABA_A$Rs.

Electrophysiology and culture of neural cells and HEK293 transfected cells. Primary culture of neurons was obtained from E18 Wistar rat embryos according to previously described procedures[76]. Briefly, neurons derived from cortical lobes were resuspended in B27 neurobasal medium plus 10% Fetal Bovine Serum (FBS) and then seeded onto poly-L-ornithine-coated (30 µg ml^{-1}) 24-well plates bearing 12-mm-diameter coverslips at 1×10^3 cells per well. The medium was replaced by serum-free B27-supplemented Neurobasal medium 24 h later. The cultures were essentially free of astrocytes and microglia and were maintained at 37 °C and 5% CO_2. Cultures were used at 7–12 days in vitro (DIV).

Primary cultures of oligodendrocytes derived from optic nerves of 12-day-old Sprague–Dawley rats were obtained as described previously[77,78]. Cells were seeded on 24-well plates bearing 12-mm-diameter coverslips coated with poly-D-lysine (10 mg ml^{-1}) at a density of 10^4 cells per well. Cells were maintained at 37 °C and 5% CO_2 in Sato medium[70] and recorded from 1 to 2 DIV.

Also, venom extracts were tested on HEK293 (human embryonic kidney) cells expressing human Na_v channels (hNa_v 1.5 or hNa_v 1.6), donated by Dr. Rita Restano Cassulini[79]. Cells were incubated in Dulbecco's modified Eagle medium (DMEM) with 10% FBS and antibiotic G418 (400 µg ml^{-1}), at 37 °C with 5% CO_2.

Whole-cell patch-clamp recordings of either neural or HEK293 membrane ionic currents were performed with an Axon 700B amplifier (Molecular Devices). Cells were constantly perfused with normal external solution (NES, containing in mM: 135 NaCl, 5 KCl, 2 $CaCl_2$, 1 $MgCl_2$, 10 HEPES, and 5 glucose adjusted at pH 7.3 with NaOH). The pipette was filled with normal internal solution (NIS, containing in mM: 5 NaCl, 130 KCl, 1 $CaCl_2$, 1.8 $MgCl_2$, 10 HEPES, 10 EGTA, 0.2 Na-GTP, and 2 Mg-ATP at pH 7.3 (KOH). Data were digitized at 5 kHz and low-pass filtered at 0.5 kHz. Currents were recorded at distinct holding membrane potentials depending on the experiment as specified in each case, digitized, and stored for analysis using the analog-to-digital converter Digidata 1400 (Molecular Devices) and pClamp10 software (Molecular Devices). Current–voltage (I–V) relationships were regularly built by changing the membrane potential from − 100 to + 40 mV in 10-mV steps of 250 ms while cells were held at − 100 mV. In some instances, cells were held at a desired membrane potential while a test solution was superfused or applied using the jet method, and the peak currents generated were I/V plotted. Time-courses of the effect on I_{Nav} were followed in cells held at − 100 mV and then depolarizing steps (20 ms) eliciting maximal current (usually to − 20 mV or − 10 mV) were applied periodically every 0.75–1 s. Usually, the control current was monitored for 10 s and then a test solution was superfused for 5–10 s to record the effect on I_{Nav}, this was followed by a washing period with NES.

In one set of experiments the action potential was recorded in neurons under current-clamp, in these cases depolarizing current pulses (0.65–0.85 nA) of 35 ms were applied to generate action potentials every 500 ms, after a recording period control, different dilutions of FII were applied to test their effect on the nerve impulse.

Dose–response curves were fitted to the equation:

$$I/I_{max} = \left[(A1 - A2)/1 + ([extract]/EC_{50})^{nH}\right] + A2,$$

by the method of nonlinear least-squares fitting, where EC_{50} is the half-maximal effective concentration for the extract, nH is the slope factor (Hill coefficient), A1 and A2 are the initial and final normalized current (I) values, respectively, and [extract] is the concentration of either FII or NE.

ELISA for GABA. GABA detection in both AE and NE was assayed using GABA ELISA Kit (Aviva Systems Biology, San Diego, CA, USA) according to the protocol instructions. Briefly, titrated standards and diluted samples were placed in a microtiter well-plate previously pre-coated with an anti-GABA antibody. GABA-Biotin complex was added to each well and the plate was incubated for 60 min. After incubation, the plate was washed. Avidin-HRP conjugate was added to each well and incubated for 45 min. Finally, 3,3′,5,5′-Tetramethylbenzidine (TMB) substrate was incubated for 30 min. Samples were read at 450 nm on an ELISA standard microplate reader.

Statistical analysis. All data are expressed as mean ± S.D. of at least 4 cells, and in the case of oocytes, cells were obtained from 2 to 7 different frogs. The means of two groups were compared using a Student's t-test, or when appropriate, by analysis of variance followed by post-hoc comparisons of individual means using the Bonferroni correction. Statistical analysis was performed using GraphPad Prism software (version 6; La Jolla, CA). Differences were considered to be significant at $p < 0.05$.

Received: 28 October 2021; Accepted: 17 March 2022
Published online: 30 March 2022

References

1. Santhanam, R. Biology of Marine Cnidarians [Phylum Cnidaria (= Coelenterata)]. In *Biology and Ecology of Venomous Marine Cnidarians* (ed. Santhanam, R.) 7–27 (Springer, 2020).
2. Brinkman, D. L. *et al.* Venom proteome of the box jellyfish *Chironex fleckeri*. *PLoS ONE* **7**, e47866 (2012).
3. Diaz-Garcia, C. M. *et al.* Toxins from *Physalia physalis* (Cnidaria) raise the intracellular Ca^{2+} of beta-cells and promote insulin secretion. *Curr. Med. Chem.* **19**, 5414–5423 (2012).
4. Remigante, A. *et al.* Impact of scyphozoan venoms on human health and current first aid options for stings. *Toxins* **10**, 133–151 (2018).
5. Fautin, D. G. Structural diversity, systematics, and evolution of cnidae. *Toxicon* **54**, 1054–1064 (2009).
6. Honma, T. & Shiomi, K. Peptide toxins in sea anemones: Structural and functional aspects. *Mar. Biotechnol.* **8**, 1–10 (2006).
7. Morabito, R., Marino, A. & La Spada, G. Nematocytes' activation in *Pelagia noctiluca* (Cnidaria, Scyphozoa) oral arms. *J. Comp. Physiol. A* **198**, 419–426 (2012).
8. Beckman, A. & Özbek, S. The nematocyst: A molecular map of the Cnidarian stinging organelle. *Int. J. Dev. Biol.* **56**, 577–582 (2012).
9. Jouiaei, M. *et al.* Ancient venom systems: A review on Cnidaria toxins. *Toxins* **7**, 2251–2271 (2015).
10. Frazão, B., Vasconcelos, V. & Antunes, A. Sea anemone (Cnidaria, Anthozoa, Actinaria) toxins: An overview. *Mar. Drugs* **10**, 1812–1851 (2012).
11. Madio, B., Undheim, E. A. B. & King, G. F. Revisting venom of the sea anemone *Stichodactyla haddoni*: Omics techniques reveal the complete toxin arsenal of a well-studied sea anemone genus. *J. Proteom.* **166**, 83–92 (2017).
12. Béress, L. & Béress, R. Purification of three polypeptides with neuro- and cardiotoxic activity from the sea anemone *Anemonia sulcata*. *Toxicon* **13**, 359–367 (1975).
13. Castañeda, O. *et al.* Characterization of a potassium channel toxin from the Caribbean sea anemone *Stichodactyla helianthus*. *Toxicon* **33**, 603–613 (1995).
14. Bruhn, T. *et al.* Isolation and characterization of five neurotoxic and cardiotoxic polypeptides from the sea anemone *Anthopleura elegantissima*. *Toxicon* **39**, 693–702 (2001).
15. Torres, M. *et al.* Electrophysiological and hemolytic activity elicited by the venom of the jellyfish *Cassiopea xamachana*. *Toxicon* **39**, 1297–1307 (2001).
16. Anderluh, G. & Maček, P. Cytolitic peptide and protein toxins from sea anemones (Anthozoa: Actinaria). *Toxicon* **40**, 111–124 (2001).
17. Marino, A., Morabito, R., Pizzata, T. & La Spada, G. Effect of various factors on *Pelagia noctiluca* (Cnidaria, Scyphozoa) crude venom-induced haemolysis. *Comp. Biochem. Physiol. A Mol. Integr. Physiol.* **151**, 144–149 (2008).
18. Lazcano-Pérez, F. *et al.* A purified *Palythoa* venom fraction delays sodium current inactivation in sympathetic neurons. *Toxicon* **82**, 112–116 (2014).
19. Morabito, R. *et al.* Crude venom from nematocysts of *Pelagia noctiluca* (Cnidaria: Scyphozoa) elicits a sodium conductance in the plasma membrane of mammalian cells. *Sci. Rep.* **7**, 41065 (2017).
20. Ames, C. L. *et al.* Cassiosomes are stinging-cell structures in the mucus of the upside-down jellyfish *Cassiopea xamachana*. *Commun. Biol.* **3**, 67 (2020).
21. Moran, Y. *et al.* Neurotoxin localization to ectodermal gland cells uncovers an alternative mechanism of venom delivery in sea anemone. *Proc. R. Soc. B* **279**, 1351–1358 (2012).
22. Columbus-Shenkar, Y. Y. *et al.* Dynamics of venom composition across a complex life cycle. *Elife* **7**, e35014 (2018).
23. Macrander, J., Broe, M. & Daly, M. Tissue-specific venom composition and differential gene expression in sea anemone. *Genome. Biol. Evol.* **8**, 2358–2375 (2016).
24. Grajales, A. & Rodríguez, E. Elucidating the evolutionary relationship of the Aiptasiidae, a widespread cnidarian-dinoflagellate model system (Cnidaria: Anthozoa: Actiniaria: Metridioidea). *Mol. Phylogenet. Evol.* **94**, 252–263 (2016).
25. Briones-Fourzán, P., Pérez-Ortiz, M., Negrete-Soto, F., Barradas-Ortiz, C. & Lozano-Álvarez, E. Ecological traits of Caribbean Sea anemones and symbiotic crustaceans. *Mar. Ecol. Prog. Ser.* **470**, 55–68 (2012).
26. González-Muñoz, R., Nuno, S., Sánchez-Rodríguez, J., Rodríguez, E. & Segura-Puertas, L. First inventory of sea anemones (Cnidaria: Actinaria) of the Mexican Caribbean. *Zootaxa* **3556**, 1–38 (2012).

27. O'Reilly, E. E. & Chadwick, N. E. Population dynamics of corkscrew sea anemones *Bartholomea annulata* in the Florida Keys. *Mar. Ecol. Prog. Ser.* **567**, 109–123 (2017).
28. Calgren, O. A survey of the Ptychodactiaria, Corallimorpharia and Actinaria. *Kungl. Svenska Vetenskapsakad. Handl.* **3**, 1–121 (1949).
29. Sánchez-Rodríguez, J., Zugasti, A., Santamaría, A., Galván-Arzate, S. & Segura-Puertas, L. Isolation, partial purification and characterization of active polypeptide from the sea anemone *Bartholomea annulata*. *Basic Clin. Pharmacol. Toxicol.* **99**, 116–121 (2006).
30. Morales-Landa, J. L. *et al.* Antimicrobial, antiprotozoal and toxic activities of cnidarian extracts from the Mexican Caribbean Sea. *Pharm. Biol.* **45**, 37–43 (2007).
31. Nesher, N. *et al.* AdE-1, a new inotropic Na^+ channel toxin from *Aiptasia diaphana*, is similar to, yet distinct from, known anemone Na^+ channel toxins. *Biochem. J.* **451**, 81–90 (2013).
32. Nesher, N., Zlotkin, E. & Hochner, B. The sea anemone toxin AdE-1 modifies both sodium and potassium currents of rat cardiomyocytes. *Biochem. J.* **461**, 51–59 (2014).
33. Lazcano-Pérez, F., Arellano, R. O., Garay, E., Arreguín-Espinosa, R. & Sánchez-Rodríguez, J. Electrophysiological activity of a neurotoxic fraction from the venom of box jellyfish *Carybdea marsupialis*. *Comp. Biochem. Physiol. C Toxicol. Pharmacol.* **191**, 177–182 (2017).
34. Bernáldez, J. *et al.* Electrophysiological characterization of a novel small peptide from the venom of *Conus californicus* that targets voltage-gated neuronal Ca^{2+} channels. *Toxicon* **57**, 60–67 (2011).
35. Parker, I., Sumikawa, K. & Miledi, R. Activation of a common effector system by different brain neurotransmitter receptors in *Xenopus Oocytes*. *Proc. R. Soc. Lond. B* **231**, 37–45 (1987).
36. Miledi, R., Parker, I. & Sumikawa, K. Transplanting receptors from brains into oocytes. In *Fidia Research Foundation Neuroscience Award Lectures*, 57–90 (Raven Press, 1989).
37. Arellano, R. O., Robles-Martínez, L., Serrano-Flores, B., Vázquez-Cuevas, F. & Garay, E. Agonist-activated Ca^{2+} influx and Ca^{2+}-dependent Cl^- channels in *Xenopus* ovarian follicular cells: Functional heterogeneity within the cell monolayer. *J. Cell. Physiol.* **227**, 3457–3470 (2012).
38. Arellano, R. O. & Miledi, R. Novel Cl- currents elicited by follicle stimulating hormone and acetylcholine in follicle-enclosed Xenopus oocytes. *J. Gen. Physiol.* **102**, 833–857 (1993).
39. Arellano, R. O., Woodward, R. M. & Miledi, R. Ion channels and membrane receptors in follicle-enclosed *Xenopus* oocytes. In *Ion Channels* Vol. 4 (ed. Narahashi, T.) 203–259 (Springer, 1996).
40. Gundersen, C. B., Miledi, R. & Parker, I. Voltage-operated channels induced by foreign messenger RNA in *Xenopus oocytes*. *Proc. R. Soc. Lond. B* **220**, 131–140 (1983).
41. Gundersen, C. B., Miledi, R. & Parker, I. Messenger RNA from human brain induces drug- and voltage-operated channels in *Xenopus* oocytes. *Nature* **308**, 421–424 (1984).
42. Bloom, D. A., Burnett, J. W. & Alderslade, P. Partial purification of box jellyfish (*Chironex fleckeri)* nematocyst venom isolated at the beachside. *Toxicon* **36**, 1075–1085 (1998).
43. Narahashi, T. Chemicals as tools in the study of excitable membranes. *Physiol. Rev.* **54**, 813–889 (1974).
44. Narahashi, T. Pharmacology of tetrodotoxin. *J. Toxicol. Toxin rev.* **20**, 67–84 (2001).
45. Lee, C. H. & Ruben, P. C. Interaction between voltage-gated sodium channels and the neurotoxin, tetrodotoxin. *Channels* **2**, 407–412 (2008).
46. Ordaz, P. R. *et al.* $GABA_A$ receptors expressed in oligodendrocytes cultured from the neonatal rat contain α3 and γ1 subunits and present differential functional and pharmacological properties. *Mol. Pharmacol.* **99**, 133–146 (2021).
47. Martínez-Torres, A. & Miledi, R. Expression of γ-aminobutyric acid ρ1 and ρ1Δ450 as gene fusion with the green fluorescent protein. *Proc. Natl. Acad. Sci. U.S.A.* **98**, 1947–1951 (2001).
48. Lazcano-Pérez, F., Hernández-Guzmán, U., Sánchez-Rodríguez, J. & Arreguín-Espinosa, R. Cnidarian neurotoxic peptides affecting central nervous system targets. *Cent. Nerv. Syst. Agents Med. Chem.* **16**, 173–182 (2016).
49. Norton, R. S. Structures of sea anemone toxins. *Toxicon* **54**, 1075–1088 (2009).
50. Iglesias-Prieto, R., Govin, N. S. & Trench, R. K. Isolation and characterization of three membrane-bound chlorophyll-protein complexes from four dinoflagellate species. *Philos. Trans. R. Soc. Lond. B* **340**, 381–392 (1993).
51. Béress, R., Béress, L. & Wunderer, G. Purification and characterisation of four polypeptides with neurotoxic activity from *Condylactis aurantiaca*. *Hope-Seyler's Z Physiol. Chem.* **357**, 409–414 (1976).
52. Rodríguez, A. A. *et al.* Peptide fingerprint of the neurotoxic fractions isolated from the secretions of sea anemone *Stichodactyla helianthus* and *Bunodosoma granulifera.* New members of the APETx-like family identified by a 454 pyrosequencing approach. *Peptides* **34**, 26–38 (2012).
53. Moran, Y., Gordon, D. & Gurevitz, M. Sea anemone toxins affecting voltage-gated sodium channels—Molecular and evolutionary features. *Toxicon* **54**, 1089–1101 (2009).
54. Madio, B., King, G. E. & Undheim, E. A. B. Sea anemone toxins: A structural overview. *Mar. Drugs* **17**, 325 (2019).
55. D'Ambra, I. & Lauritano, C. A. Review of toxins from Cnidaria. *Mar. Drugs* **18**, 507 (2020).
56. Aneiros, A. *et al.* A potassium channel toxin from the secretion of the sea anemone *Bunodosoma granulifera.* Isolation, amino acid sequence and biological activity. *Biochim. Biophys. Acta* **1157**, 86–92 (1993).
57. Ständker, L. *et al.* A new toxin from the sea anemone *Condylactis gigantea* with effect on sodium channel inactivation. *Toxicon* **48**, 211–220 (2006).
58. Zaharenko, A. J. *et al.* Characterization of selectivity and pharmacophores of type 1 sea anemone toxins by screening seven Na_v sodium channel isoforms. *Peptides* **34**, 158–167 (2012).
59. Liao, Q., Feng, Y., Yang, B. & Lee, S.-Y. Cnidarian peptide neurotoxins: A new source of various ion channel modulators or blockers against central nervous system disease. *Drug Discov. Today* **24**, 189–197 (2019).
60. Catteral, W. A. & Béress, L. Sea anemone toxin and scorpion toxin share a common receptor site associated with the action potential sodium ionophore. *J. Biol. Chem.* **253**, 7393–7396 (1978).
61. Ahern, C. A., Payandeh, J., Bosman, F. & Chanda, B. The hitchhiker's guide to the voltage-gated sodium channel galaxy. *J. Gen. Physiol.* **147**, 1–24 (2016).
62. Ravindran, V. S., Kannan, L. & Venkateshvaran, K. Biological activity of sea anemone proteins: I. Toxicity and histopathology. *Indian J. Exp. Biol.* **47**, 1225–1232 (2010).
63. Israel, M. R., Tay, B., Deuis, J. R. & Vetter, I. Sodium channels and venom peptide pharmacology. *Adv. Pharmacol.* **127**, 87–108 (2017).
64. Dudley, S. C. *et al.* μ-Conotoxin GIIIA interactions with the voltage-gated Na^+ channel predict a clockwise arrangement of the domains. *J. Gen. Physiol.* **116**, 679–689 (2000).
65. Kubota, T., Dang, B., Carvalho-de-Souza, J. L., Correa, A. M. & Benzanilla, F. Nav channel binder containing a specific conjugation-site based on a low toxicity β-scorpion toxin. *Sci. Rep.* **7**, 16329 (2017).
66. Hernández-Plata, E. *et al.* Overexpression of Nav 1.6 channels is associated with the invasion capacity of human cervical cancer. *Int. J. Cancer* **130**, 2013–2023 (2012).
67. Israel, M. R., Morgan, M., Tay, B. & Deuis, J. R. Toxins as tools: Fingerprinting neuronal pharmacology. *Neurosci. Lett.* **679**, 4–14 (2018).

68. Kozlov, S. Animal toxins for channelopathy treatment. *Neuropharmacology* **132**, 83–97 (2018).
69. Jayathilake, J. M. N. J. & Gunathilake, K. V. K. Cnidarian toxins: Recent evidences for potential therapeutic uses. *Eur. Zool. J.* **87**(1), 708–713 (2020).
70. Johnston, G. A. R. Muscimol as an ionotropic GABA receptor agonist. *Neurochem. Res.* **39**, 1942–1947 (2014).
71. Kudryavtsev, D. S. *et al.* Neurotoxins from snake venoms and α-conotoxin ImI inhibit functionally active ionotropic γ-aminobutyric acid (GABA) receptors. *J. Biol. Chem.* **290**, 22747–22758 (2015).
72. Scappaticci, A. A. & Kass-Simon, G. NMDA and $GABA_B$ receptors are involved in controlling nematocyst discharge in hydra. *Comp. Biochem. Physiol. A* **150**, 415–422 (2008).
73. Chomczynski, P. & Sacchi, N. Single-step method of RNA isolation by acid guanidinium thiocyanate-phenol-chloroform extraction. *Anal. Biochem.* **162**, 156–159 (1987).
74. Dumont, J. N. Oogenesis in *Xenopus laevis* (Daudin). I. Stages of oocyte development in laboratory maintained animals. *J. Morphol.* **136**, 153–179 (1972).
75. Pérez-Samartín, A. *et al.* Inwardly rectifying K^+ currents in cultured olidendrocytes from rat optic nerve are insensitive to pH. *Neurochem. Res.* **42**, 2443–2455 (2017).
76. Cisneros-Mejorado, A. *et al.* Demyelination-remyelination of the rat caudal cerebellar peduncle evaluated with magnetic resonance imaging. *Neuroscience* **439**, 255–267 (2020).
77. Barres, B. A. *et al.* Cell death and control cell survival in the oligodendrocyte lineage. *Cell* **70**, 31–46 (1992).
78. Arellano, R. O. *et al.* Axon-to-glia interaction regulates $GABA_A$ receptor expression in oligodendrocytes. *Mol. Pharmacol.* **89**, 63–74 (2016).
79. Restano-Cassulini, R., Garcia, W., Paniagua-Solís, J. E. & Possani, L. D. Antivenom evaluation by electrophysiological analysis. *Toxins* **9**, 74 (2017).

Acknowledgements

The authors are grateful to M.Sc. Sergio Wendoline, M.Sc. Amanda Pérez, M.Sc. Edgar Escalante and Mr. Amaury Mendoza for their help in *B. annulata* collection, and to Mr. Yamir Sánchez for *B. annulata* photographs. Dr. Arisaí C. Hernández-Sámano, Dr. Raúl Castillo-Medina, Exp. Biol. Andrés Falcón, M.Sc. Laura Celis, M.Sc. Aleida Flores-Pérez and C. Luisa Fernanda Cruz for their invaluable technical support. Dr. Roberto Arreguín-Espinosa and M.Sc. Lucero Rios Ruiz from Instituto de Química, UNAM, for their help with mass spectrometry analysis. This study was supported by Grants from PAPIIT-UNAM-México No. IN217420 to J.S.-R., No. IN203519 to R.O.A., No. IN208617 to M.B.A., and CONACyT No. 1771 to A.C.-M. (Cátedras-CONACYT Researcher). A.C.-C. is a doctoral student from Posgrado de Ciencias del Mar y Limnología at Universidad Nacional Autónoma de México (UNAM) and received CONACyT No. 517866 and PAPIIT No. IN217420 scholarships.

Author contributions

A.C.-C., J.S.-R., R.O.A. and M.B.A. participated in research design. A.C.-C., J.S.-R., R.O.A., E.G., and A.C.-M. conducted experiments. A.C.-C., J.S.-R., R.O.A., E.G., A.C.-M., M.B.A. and F.L.-P. wrote or contributed to the writing of the manuscript. All authors analyzed the results and critically commented on the manuscript.

Competing interests

The authors declare no competing interests.

Additional information

Supplementary Information The online version contains supplementary material available at https://doi.org/10.1038/s41598-022-09339-x.

Correspondence and requests for materials should be addressed to R.O.A. or J.S.-R.

Reprints and permissions information is available at www.nature.com/reprints.

Publisher's note Springer Nature remains neutral with regard to jurisdictional claims in published maps and institutional affiliations.